



Bifurcation indicator for geometrically nonlinear elasticity using the Method of Fundamental Solutions

Omar Askour^a, Abdeljalil Tri^{b,c}, Bouazza Braikat^{a,*}, Hamid Zahrouni^{d,e}, Michel Potier-Ferry^{d,e}

^a Laboratoire d'ingénierie et matériaux (LIMAT), Faculté des sciences Ben M'Sik, Hassan II University of Casablanca, BP 7955, Sidi Othman, Casablanca, Morocco

^b Institut supérieur des études maritimes (ISEM), Km 7, route d'El Jadida, Casablanca, Morocco

^c Laboratoire de mécanique, Faculté des sciences Ain Chok, Hassan II University of Casablanca, Casablanca, Morocco

^d Université de Lorraine, CNRS, Arts et Métiers ParisTech, LEM3, 57000 Metz, France

^e DAMAS, Laboratory of Excellence on Design of Alloy Metals for low-mAss Structures, Université de Lorraine, 57000 Metz, France



ARTICLE INFO

Article history:

Received 16 November 2018

Accepted 7 January 2019

Available online 21 January 2019

Keywords:

Bifurcation indicator

Method of Fundamental Solutions

Asymptotic Numerical Method

Nonlinear computation

ABSTRACT

In the present work, we propose a numerical analysis of instability and bifurcations for geometrically nonlinear elasticity problems. These latter are solved by using the Asymptotic Numerical Method (ANM) associated with the Method of Fundamental Solutions (MFS). To compute bifurcation points and to determine the critical loads, we propose three techniques. The first one is based on a geometrical indicator obtained by analyzing the Taylor series. The second one exploits the properties of the Padé approximants, and the last technique uses an analytical bifurcation indicator. Numerical examples are studied to show the efficiency and the reliability of the proposed algorithms.

© 2019 Académie des sciences. Published by Elsevier Masson SAS. All rights reserved.

1. Introduction

Bifurcation and buckling are instability phenomena very common in structural mechanics, which occur when the load reaches a critical value, leading to large deformations or to collapse of the structure. Consequently, it is necessary to develop numerical tools to predict this critical loading.

The main objective of this work consists in associating the Method of Fundamental Solutions (MFS) with the Asymptotic Numerical Method (ANM) to solve large-strain elasticity problems and to compute bifurcation points.

ANM consists in expanding the unknowns of nonlinear problems into Taylor series with respect to a path parameter. This allows one to transform the nonlinear problem into a sequence of linear ones that can be solved by using the classical finite element method or a meshless method [1–3]. A large part of the asymptotic solution is obtained analytically with high accuracy inside the validity range of the Taylor series. To improve this validity range, Padé approximants can be used. It consists in transforming the polynomial series into rational fractions having the same denominator [2,4]. To compute the entire response curve, a continuation procedure is needed to obtain the solution in a step-by-step manner. The step length, computed a posteriori, is adaptive and depends on the local nonlinearity of the response branch [1]. ANM has been successfully applied in nonlinear solid mechanics and fluid mechanics [3,5] and extended to instability analysis in

* Corresponding author.

E-mail address: b.braikat@gmail.com (B. Braikat).

solid and fluid mechanics by using bifurcation indicators well adapted to ANM. Three techniques are used to detect the bifurcation points. The first method permits to determine the singular points geometrically by localizing zones of asymptotic step accumulations. The root of the denominator of the Padé approximants represents the second technique of computing bifurcation. The third method consists in computing a scalar bifurcation indicator, along the nonlinear solution branches, which is null at the singular points. Generally, the ANM algorithm is associated with the classical finite element method. Recently, this technique has been combined with a meshless method and particularly with the Method of Fundamental Solutions [1,6].

MFS is a meshless method introduced by Kupradze and Aleksidze [7]. It has been proven to be an effective method for problems where the fundamental solutions are available [8]. For non-homogeneous problems, Radial Basis Functions (RBF) are used [9]. For elasticity problems, Marin et al. [10] have applied MFS to solve two-dimensional linear Cauchy problem. Karageorghis et al. [11] have studied the inverse problem of the coupled thermo-elasticity in the static regime. Naffa et al. [12] have used a classical iterative method associated with RBF to solve large deflection problem of thin plates. More recently, elastic-plastic deformation of plate has been studied by combining the incremental technique with meshless methods [13]. Askour et al. [6] have associated MFS with ANM to solve nonlinear elasticity problems. They have shown that this technique is efficient to compute nonlinear response curves. The present work represents an extension of this algorithm to predict instability phenomena in structural mechanics. We are mainly interested in buckling by applying the bifurcation indicators presented before. We note that we have already presented these algorithms for eigenvalue problems governed by nonlinear Poisson’s equations [2].

The present paper is organized as follows. In section 2, governing equations of nonlinear elasticity problem are formulated. In section 3, the principle of ANM is presented and applied to the geometrically nonlinear elasticity problem. Section 4 details bifurcation indicators based on Taylor series. Section 5 explains how to use Padé approximants to compute bifurcation points. In section 6, we present the principle of MFS and its application to the nonlinear elasticity problem. In the last section, numerical examples are studied to show the effectiveness of the proposed algorithm and the work is achieved by a conclusion.

2. Problem formulation

We consider a domain Ω with an external boundary $\partial\Omega$ describing the structure at a reference state. This structure is subjected to prescribed displacements U^d and traction T^d on the disjointed complementary parts of the boundary $\partial\Omega_u$ (Dirichlet boundaries) and $\partial\Omega_f$ (Neumann boundaries). Large strains are considered and a Lagrangian formulation is adopted. The equilibrium equations by neglecting the body forces associated with the boundary conditions are defined as follows:

$$\begin{cases} \nabla \cdot \Pi = 0 & \text{in } \Omega \\ \Pi \cdot n = \lambda T^d & \text{over } \partial\Omega_f \\ U = U^d & \text{over } \partial\Omega_u \end{cases} \tag{1}$$

where Π is the first Piola–Kirchhoff stress tensor associated with a point in its reference configuration, n is the outward unit normal vector to $\partial\Omega$, λ is a scalar parameter, and U denotes the displacement field. Moreover, we assume that the material is elastic, homogeneous, and isotropic, that the constitutive relation is linear. We take into account the geometric nonlinearities that can be written under the following form:

$$S = C : \gamma \tag{2}$$

where C represents the fourth-order elastic tensor, S is the second Piola–Kirchhoff stress tensor, which is linked to the first Piola–Kirchhoff stress tensor Π by the relation:

$$\Pi = FS \tag{3}$$

the tensor γ represents the Green–Lagrange strain tensor defined by:

$$\gamma = \frac{1}{2}({}^tFF - I) \tag{4}$$

such that F is the transformation gradient tensor defined by $F = \nabla U + I$ and I is the second-order identity tensor. Equations (3) and (4) can be written under the following simple form:

$$\begin{cases} \gamma = \mathcal{L}^\gamma(U) + \mathcal{Q}^\gamma(U, U) \\ \Pi = \mathcal{L}^\Pi(S) + \mathcal{Q}^\Pi(U, S) \end{cases} \tag{5}$$

where $\mathcal{L}^*(\cdot)$ represents a linear operator and $\mathcal{Q}^*(\cdot, \cdot)$ a quadratic one. Equations (1), (2) and (5) constitute the strong formulation of the boundary value problem. We collect all the unknowns into a single unknown vector $\{\mathbb{U}\} = \langle \Pi, S, \gamma, U \rangle$.

3. Computation of the solution branch by ANM

The basic idea of ANM consists in searching the solution path to the nonlinear problem (1), (2) and (5) under an asymptotic expansion form with respect to a control parameter a . This expansion is developed in the neighborhood of a known regular solution $(\mathbb{U}_0, \lambda_0)$,

$$\begin{Bmatrix} \mathbb{U} \\ \lambda \end{Bmatrix} = \begin{Bmatrix} \mathbb{U}_0 \\ \lambda_0 \end{Bmatrix} + \sum_{k=1}^p a^k \begin{Bmatrix} \mathbb{U}_k \\ \lambda_k \end{Bmatrix} \tag{6}$$

where p is the truncation order of the asymptotic expansions. The control parameter a can be defined as:

$$a = \langle U - U_0, U_1 \rangle + (\lambda - \lambda_0)\lambda_1 \tag{7}$$

with $\langle \cdot, \cdot \rangle$ denotes the Euclidean scalar product. Equation (7) provides an adaptive path parameter a , which can be identified with an arc-length parameter. By substituting (6) into (1), (2), (5) and (7) and equating the coefficients of the same power of a , one transforms the nonlinear problem into a sequence of linear ones as follows.

Order 1:

$$\begin{cases} \gamma_1 & = \mathcal{L}^\gamma(U_1) + 2\mathcal{Q}^\gamma(U_0, U_1) & \text{in } \Omega \\ S_1 & = C : \gamma_1 & \text{in } \Omega \\ \Pi_1 & = \mathcal{L}^\Pi(S_1) + \mathcal{Q}^\Pi(U_0, S_1) + \mathcal{Q}^\Pi(U_1, S_0) & \text{in } \Omega \\ \mathcal{L}_t^\nabla(U_1) & = 0 & \text{in } \Omega \\ \mathcal{L}_t^f(U_1) & = \lambda_1 T^d & \text{over } \partial\Omega_f \\ U_1 & = 0 & \text{over } \partial\Omega_u \\ \langle U_1, U_1 \rangle + \lambda_1^2 & = 1 & \text{in } \Omega \end{cases} \tag{8}$$

Order k (with $2 \leq k \leq p$):

$$\begin{cases} \gamma_k & = \mathcal{L}^\gamma(U_k) + 2\mathcal{Q}^\gamma(U_0, U_k) + \sum_{r=1}^{k-1} \mathcal{Q}^\gamma(U_r, U_{k-r}) & \text{in } \Omega \\ S_k & = C : \gamma_k & \text{in } \Omega \\ \Pi_k & = \mathcal{L}^\Pi(S_k) + \mathcal{Q}^\Pi(U_0, S_k) + \mathcal{Q}^\Pi(U_k, S_0) + \sum_{r=1}^{k-1} \mathcal{Q}^\Pi(U_r, S_{k-r}) & \text{in } \Omega \\ \mathcal{L}_t^\nabla(U_k) & = \mathcal{Q}_k^\nabla & \text{in } \Omega \\ \mathcal{L}_t^f(U_k) & = \lambda_k T^d + \mathcal{Q}_k^f & \text{over } \partial\Omega_f \\ U_k & = 0 & \text{over } \partial\Omega_u \\ \langle U_k, U_1 \rangle + \lambda_k \lambda_1 & = 0 & \text{in } \Omega \end{cases} \tag{9}$$

The tangent operators are denoted by \mathcal{L}_t^∇ and \mathcal{L}_t^f , which depend on the initial solution \mathbb{U}_0 , the operators denoted by \mathcal{Q}_k^∇ and \mathcal{Q}_k^f are the quadratic ones, which depend on the solutions computed at the previous orders. Finally, all vectors \mathbb{U}_k and the scalar parameters λ_k of series (6) can be determined by solving the system of Eqs. (8) and (9) at each truncation order. We recall that all the linear problems (8) and (9) have the same tangent operator and different forms of right-hand sides. In fact, only one matrix decomposition in each ANM-step is needed. The expressions of these operators are given in the appendix.

The validity range of the series (6) is limited by the convergence radius. To obtain the whole solution branch, a continuation technique is used. It consists in computing the step length of the solution automatically by the following formula [5]:

$$a_{\max} = \left(\varepsilon \frac{\|U_1\|}{\|U_p\|} \right)^{\frac{1}{p-1}} \tag{10}$$

Here, ε is a small number and the norm $\|\cdot\|$ in (10) is chosen as the Euclidean norm. The solution $\{\mathbb{U}(a_{\max}), \lambda(a_{\max})\}$ is a new starting solution for the following step. This technique allows us to compute a posteriori the step length of the solution, which is naturally adaptive and depends on the local nonlinearity of the considered problem.

Indeed, in a neighborhood of a bifurcation point, we observe step accumulations that are considered as geometrical indicators of singular points. In the following sections, we will be interested in developing a second indicator, well adapted to the framework of ANM, and a third one based on Padé approximants.

4. Bifurcation indicator based on Taylor series

In this section, we define a scalar bifurcation indicator well adapted to ANM, which is obtained by introducing a fictitious perturbation in the problem. By evaluating this indicator through the equilibrium branch, the critical points and the associated bifurcation modes can be determined.

Let $\delta\mu f_\mu$ be a fictitious perturbation force applied to the structure at a given deformed state, where f_μ is a random function and $\delta\mu$ is the unknown intensity of the perturbation. The primary solution \mathbb{U} is then perturbed by the fluctuation $\delta\mathbb{U}$. By superposing the perturbation and the applied load, the fictitious perturbed equilibrium is described by

$$\begin{cases} \nabla \cdot (\Pi + \delta\Pi) = 0 & \text{in } \Omega \\ (\Pi + \delta\Pi) \cdot n = \lambda T^d + \delta\mu f_\mu & \text{over } \partial\Omega_f \\ (U + \delta U) = U^d & \text{over } \partial\Omega_u \end{cases} \quad (11)$$

Considering the equilibrium state and taken into account Eq. (2) and (5) and neglecting the quadratic terms, we obtain the following perturbed problem:

$$\begin{cases} \delta\gamma = \mathcal{L}^\gamma(\delta U) + 2\mathcal{Q}^\gamma(U, \delta U) & \text{in } \Omega \\ \delta S = C : \delta\gamma & \text{in } \Omega \\ \delta\Pi = \mathcal{L}^\Pi(\delta S) + \mathcal{Q}^\Pi(U, \delta S) + \mathcal{Q}^\Pi(\delta U, S) & \text{in } \Omega \\ \nabla \cdot \delta\Pi = 0 & \text{in } \Omega \\ \delta\Pi \cdot n = \delta\mu f_\mu & \text{over } \partial\Omega_f \\ \delta U = 0 & \text{over } \partial\Omega_u \end{cases} \quad (12)$$

To obtain a well-posed problem, the following equation is added to system (12):

$$\langle \delta U - \delta U_0, \delta U_0 \rangle = 0 \quad (13)$$

The initial fluctuation δU_0 is a solution to the perturbed problem for $\delta\mu = 1$. Bifurcation points correspond to the zero of the function $\delta\mu(\lambda)$. Unknowns of the resulting system ($\delta\mathbb{U}$ and $\delta\mu$) are developed in Taylor series according to the path parameter a :

$$\begin{Bmatrix} \delta\mathbb{U} \\ \delta\mu \end{Bmatrix} = \begin{Bmatrix} \delta\mathbb{U}_0 \\ \delta\mu_0 = 1 \end{Bmatrix} + \sum_{k=1}^p a^k \begin{Bmatrix} \delta\mathbb{U}_k \\ \delta\mu_k \end{Bmatrix} \quad (14)$$

where $\delta\mathbb{U}_0$ and $\delta\mu_0$ are the initial solution to the perturbed problem. By introducing Eqs. (6) and (14) into (12) and (13) and by identifying according to the powers of a , we obtain a series of following linear problems.

Order 0:

$$\begin{cases} \delta\gamma_0 = \mathcal{L}^\gamma(\delta U_0) + 2\mathcal{Q}^\gamma(U_0, \delta U_0) & \text{in } \Omega \\ \delta S_0 = C : \delta\gamma_0 & \text{in } \Omega \\ \delta\Pi_0 = \mathcal{L}^\Pi(\delta S_0) + \mathcal{Q}^\Pi(U_0, \delta S_0) + \mathcal{Q}^\Pi(\delta U_0, S_0) & \text{in } \Omega \\ \mathcal{L}_t^\nabla(\delta U_0) = 0 & \text{in } \Omega \\ \mathcal{L}_t^f(\delta U_0) = \delta\mu_0 f_\mu & \text{over } \partial\Omega_f \\ \delta U_0 = 0 & \text{over } \partial\Omega_u \end{cases} \quad (15)$$

Order k (with $1 \leq k \leq p$):

$$\begin{cases}
 \delta\gamma_k & = \mathcal{L}^\gamma(\delta U_k) + 2\mathcal{Q}^\gamma(U_0, \delta U_k) + \sum_{r=1}^k 2\mathcal{Q}^\gamma(U_r, \delta U_{k-r}) & \text{in } \Omega \\
 \delta S_k & = C : \delta\gamma_k & \text{in } \Omega \\
 \delta\Pi_k & = \mathcal{L}^\Pi(\delta S_k) + \mathcal{Q}^\Pi(U_0, \delta S_k) + \mathcal{Q}^\Pi(\delta U_k, S_0) + \sum_{r=1}^k \mathcal{Q}^\Pi(U_r, \delta S_{k-r}) + \mathcal{Q}^\Pi(\delta U_{k-r}, S_r) & \text{in } \Omega \\
 \mathcal{L}_t^\nabla(\delta U_k) & = \delta\mathcal{Q}_k^\nabla & \text{in } \Omega \\
 \mathcal{L}_t^f(\delta U_k) & = \delta\mu_k f_\mu + \delta\mathcal{Q}_k^f & \text{over } \partial\Omega_f \\
 \delta U_k & = 0 & \text{over } \partial\Omega_u \\
 \langle \delta U_k, \delta U_0 \rangle & = 0 & \text{in } \Omega
 \end{cases} \tag{16}$$

The vectors \mathbb{U}_k are already determined during the computation of the equilibrium branch. It will be noted that the resultant linear problems (15) and (16) have the same tangent operators ($\mathcal{L}_t^\nabla, \mathcal{L}_t^f$) computed for the equilibrium branch (8) and (9) and differ only by their right-hand sides ($\delta\mathcal{Q}_k^\nabla, \delta\mathcal{Q}_k^f$), which are given in the appendix. The bifurcation points correspond to the values of the parameter $\lambda = \lambda_{\text{critical}}$ for which the function $\delta\mu(\lambda_{\text{critical}})$ vanishes. The bifurcation mode is given by the corresponding vector $\delta U(\lambda_{\text{critical}})$.

5. Bifurcation indicator based on Padé approximants

The Padé approximants [14] consist in transforming polynomial series into rational fractions, which permits to improve the validity range of the series. Indeed, Eq. (6) is replaced by the following representation:

$$\begin{cases}
 \begin{Bmatrix} \mathbb{U} \\ \lambda \end{Bmatrix} = \begin{Bmatrix} \mathbb{U}_0 \\ \lambda_0 \end{Bmatrix} + \sum_{k=1}^{p-1} f_k[a] a^k \begin{Bmatrix} \mathbb{U}_k \\ \lambda_k \end{Bmatrix} \\
 f_k[a] = \frac{P_{p-k-1}[a]}{P_{p-1}[a]}
 \end{cases} \tag{17}$$

where $f_k[a]$ are rational fractions admitting the same denominator and $P_k[a]$ is a polynomial in a of degree k . This representation has been introduced in reference [4]. A simple method to detect bifurcation points can be established by analyzing a posteriori the rational representation (17). It has been early recognized that a bifurcation point corresponds to a real root of the denominator of the fraction $f_k[a]$ [2].

6. The Method of Fundamental Solutions

In this section, we propose to discretize linear Eqs. (8), (9), (15), and (16) using the MFS-RBF method [6]. The principle of this method consists in searching the unknowns of the problem in the form of a superposition of homogeneous and particular solutions. The homogeneous solution is defined as a linear combination of the fundamental solutions in terms of the source points located outside the domain. The computation of a particular solution is based on Radial Basis Functions (RBF) in terms of the collocation points. The Analogous Equations Method (AEM) [15] is used to transform the resulting linear Eqs. (8), (9), (15), and (16) into a system of equations for which the linear operator of two-dimensional elasticity is available [2]. To facilitate the comprehension, we use the MFS-RBF to solve only the system (9), which has the same generic form as the problems (8), (15), and (16). For that, we search the unknowns U as follows:

$$\{U(M_i)\} = \sum_{j=1}^{N_s} [\widehat{U}h^h(M_i, Q_j)] \begin{Bmatrix} \alpha_j h^h \\ \beta_j h^h \end{Bmatrix} + \sum_{j=1}^N [\widehat{U}^{\text{par}}(M_i, M_j)] \begin{Bmatrix} \alpha_j^{\text{par}} \\ \beta_j^{\text{par}} \end{Bmatrix} \tag{18}$$

where $Q_j(X_1^j, X_2^j)$ and $M_i(x_1^i, x_2^i)$ are respectively the coordinates of the N_s source points and the coordinates of the N collocation points.

$[\widehat{U}h^h(M_i, Q_j)]$ represents the matrix of fundamental solutions to the two-dimensional linear elasticity operator. These fundamental solutions are given by the following formula [10]:

$$\widehat{U}_{kl}h^h(r_{ij}) = \frac{-r_{ij}^2}{8\pi\mu(1-\nu)} \left((3-4\nu)\log(r_{ij})r_{ij}^2\delta_{kl} - (x_k^i - x_k^j)(x_l^i - x_l^j) \right) \tag{19}$$

where k and l vary between 1 and 2, and r_{ij} represents the distance between the collocation point M_i and the source points Q_j taken on a fictitious boundary Γ_f containing the domain Ω , whereas the matrix $[\widehat{U}^{\text{par}}(M_i, M_j)]$ of the particular

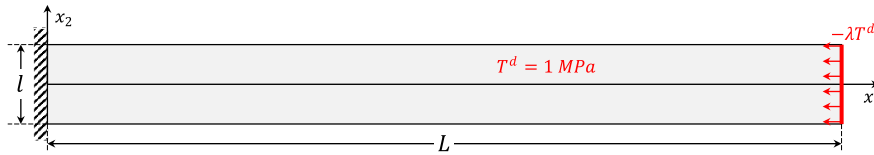


Fig. 1. Buckling of a thin plate.

solution is built from the Radial Basis Functions [16]. The efficiency and accuracy of the approximation are conditioned by the judicious choice of the Radial Basis Function (RBF). Here, the multi-quadrics RBF type is considered. Thereafter, it is proposed to rewrite expression (18) in a compact form in which the matrices of the particular and homogeneous solutions are concatenated in a single matrix $[\widehat{U}]$ and the coefficients of linear combinations $\alpha_j h^h$, $\beta_j h^h$, α_j^{par} and β_j^{par} are collected into a single vector $\{X\}$ in the following form:

$$\{U(M_i)\} = [\widehat{U}(M_i)]\{X\} \tag{20}$$

By introducing the approximation (20) into the set of Eqs. (9), we obtain a linear algebraic system at a truncation order k ($2 \leq k \leq p$), which is written under the following form:

$$[K_T]\{X_k\} = \lambda_k \{F\} + \{F_k^{nl}\} \tag{21}$$

where $[K_T]$, F_k^{nl} and F are respectively given by:

$$[K_T] = \begin{bmatrix} \mathcal{L}_t^\nabla([\widehat{U}(M_i)]) \\ \mathcal{L}_t^f([\widehat{U}(M_i)]) \\ [\widehat{U}(M_i)] \end{bmatrix}; \{F_k^{nl}\} = \begin{Bmatrix} \{Q_k^\nabla\} \\ \{Q_k^f\} \\ \{0\} \end{Bmatrix}; \{F\} = \begin{Bmatrix} \{0\} \\ \{T^d\} \\ \{0\} \end{Bmatrix} \tag{22}$$

We denote by N_f the number of collocation points on the boundary $\partial\Omega$. The system (21) is of order $2((N + N_f) \times (N_s + N))$. To have a unique solution, N_s and N_f must satisfy the following inequality $N_s \leq N_f$. Generally, we assumed that the number of source points N_s is equal to the number of collocation points on the boundary N_f .

7. Numerical results and discussions

The first example deals with buckling of an elastic and homogeneous thin plate having a length $L = 100$ mm, a width $l = 10$ mm, and a thickness $h = 1$ mm. The characteristics of the material are Young’s modulus $E = 10$ GPa and Poisson’s ratio $\nu = 0.3$. The plate is embedded at its left edge and subjected to an axial compressive load λT^d as shown in Fig. 1. In this study, we are interested in the first bifurcated branch, which is symmetric and stable.

For numerical data, we adopt $N = 467$ collocation points arbitrarily distributed on the domain occupied by the plate and $N_s = 113$ source points on the fictitious boundary, which is considered as a circle of radius $R = 70$ mm and of center $(x_1 = 50, x_2 = 0)$. The optimal shape parameter of the multi-quadrics RBF $(\sqrt{r^2 + c^2})$ is given by the best residual. According to numerical tests, we chose the shape parameter as $c = 0.03$. We use the TSVD method as a regularization method with a GCV-type criterion for the choice of the optimal regularization parameter. In a recent paper [6], we have analyzed and discussed the influence of different parameters of the proposed algorithm (MFS-ANM) as well as different regularization methods. The Asymptotic Numerical Method has been applied with a truncation order $p = 15$ and a tolerance parameter $\varepsilon = 10^{-6}$. The results of the MFS-ANM algorithm will be compared with those given by FEM-ANM.

For the analysis of MFS-ANM parameters, the reader can refer to the work of Tri et al. [2]. To assess the validity of the proposed algorithm, the results of MFS-ANM are compared to those obtained with finite element code FEM-ANM. In Figs. 2a and 2b, the response curves are reported at point $(x_1 = 100, x_2 = 5)$ for components U_1 and U_2 , respectively. To follow the bifurcated branch, a small perturbation load is introduced in the initial problem. In Fig. 2a, one observes two branches. The first one corresponds to the fundamental branch that switches with the bifurcated one in the neighborhood of the bifurcation point. In this area appear step accumulations of the continuation asymptotic solution, which represents a geometrical indicator of the bifurcation point. The FEM-ANM algorithm requires a time CPU greater than this of the proposed algorithm MFS-ANM to compute the whole solution. For this solution, the FEM-ANM algorithm requires a CPU time 729.22 s, but the MFS-ANM algorithm only requires 97.32 s. The bifurcation point is then located geometrically and corresponds to the critical load $\lambda_c = 20.50$. Since the bifurcation is symmetrical, to obtain the two bifurcated branches one change the sign of the perturbation load. Indeed, in Fig. 2b, these two branches are separated near the critical value.

This critical point can also be computed by using the bifurcation indicator given by Eq. (11). To this end, we introduce a random fictitious perturbation force f_μ given in Eq. (11). The variations of the scalar function $\delta\mu$ versus the load parameter λ are reported in Fig. 3 for different truncation orders of the Taylor series. We observe that the three curves are null inside their validity range and for $\lambda_c = 20.50$, which correspond to the value obtained by using the geometrical indicator described previously.

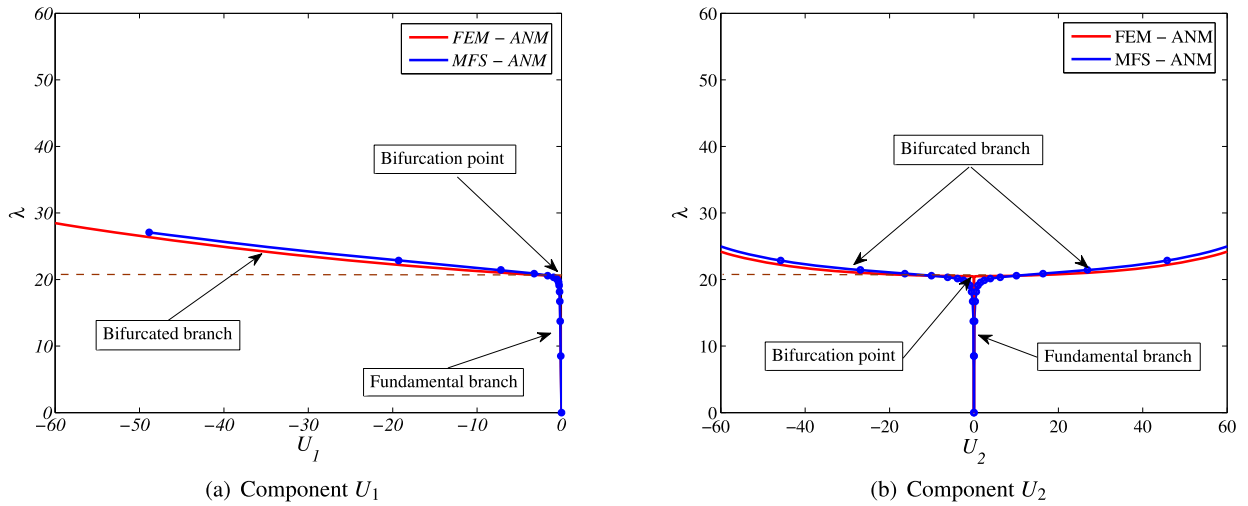


Fig. 2. Solution branches at point $(x_1 = 100, x_2 = 5)$ by the MFS-ANM-Continuation technique and by FEM-ANM-Continuation technique.

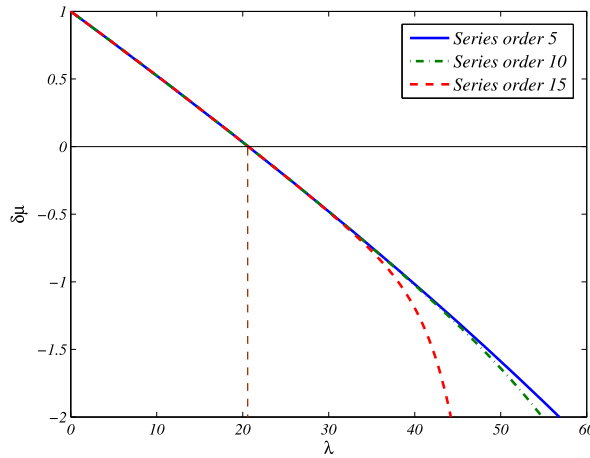


Fig. 3. Bifurcation indicator $\delta\mu$, along the fundamental branch, as a function of the load parameter λ .

Table 1
Bifurcation indicator using Taylor series and the denominator of the Padé approximants for different truncation orders.

		$p = 5$	$p = 10$	$p = 15$
$\varepsilon = 10^{-2}$	Bifurcation indicator by Taylor series	20.5089	20.5087	20.5088
	Bifurcation indicator by Padé approximants	20.4966	20.4966	20.4966
$\varepsilon = 10^{-6}$	Bifurcation indicator by Taylor series	20.5089	20.5087	20.5088
	Bifurcation indicator by Padé approximants	20.4966	20.4966	20.4966

The second indicator is based on Padé approximants. Indeed, by transforming the Taylor series into rational fractions, one obtains directly the bifurcation point by computing the first real root denominator of these fractions [2]. In Table 1, we report the critical load obtained by the polynomial and the Padé approximants indicators for different truncation orders p and different accuracy parameters ε . We remark that, for this example, the critical load is not sensitive to these parameters. In other words, the indicator based on the Taylor series (14) and the pole of the Padé approximants (17) give the same value as the geometrical one. This result confirms the effectiveness of our algorithms in computing bifurcation points.

We consider a second example, which deals with the buckling of a simple supported plate subjected to axial compression as shown in Fig. 4. For symmetry reasons, only a half of the structure is considered. The three techniques to detect bifurcations are applied.

In Fig. 5a, we have plotted the evolution of the displacement U_2 versus the load parameter λ . A numerical solution obtained with the proposed MFS-ANM algorithm is compared with the FEM-ANM one. The bifurcation point is localized

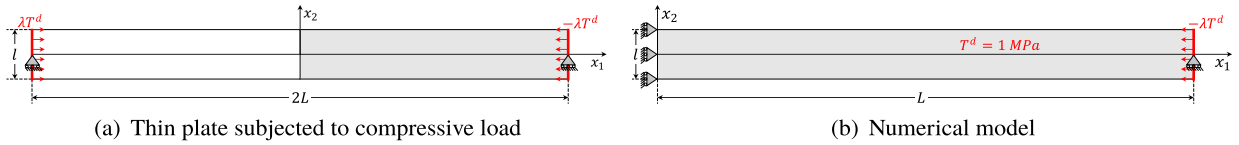


Fig. 4. Buckling of a thin plate subjected to compressive load and its numerical model.

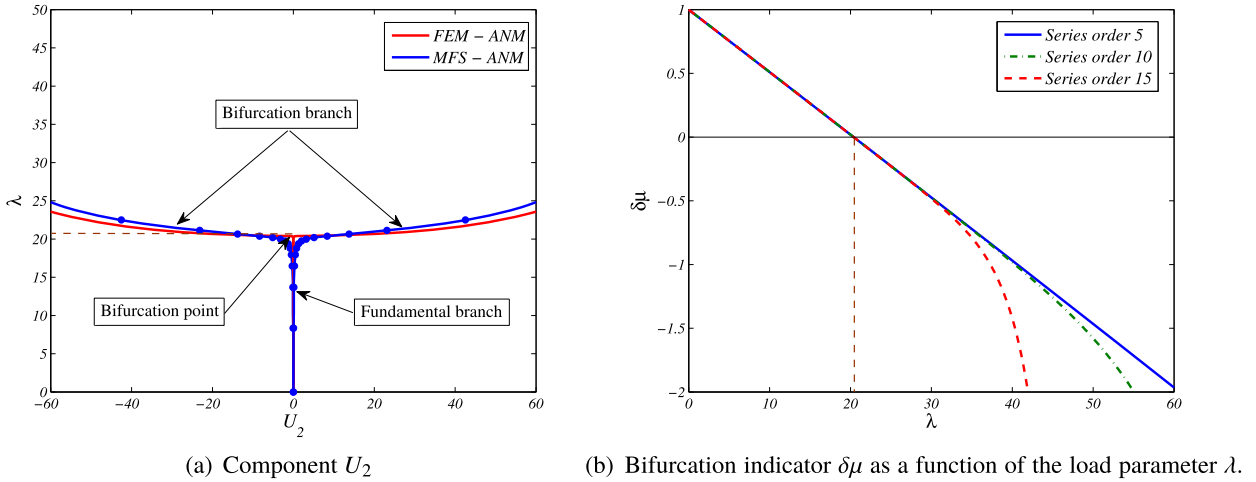


Fig. 5. Solution branches at point $(x_1 = 0, x_2 = 5)$ by the MFS-ANM-Continuation technique and by FEM-ANM-Continuation technique. Bifurcation indicator $\delta\mu(\lambda)$.

Table 2
Bifurcation indicator using series expansion and the denominator of Padé approximant for different truncation orders.

	$p = 5$	$p = 10$	$p = 15$
Bifurcation indicator by Taylor series	20.3885	20.3886	20.3887
Bifurcation indicator by Padé approximants	20.3795	20.3795	20.3795

geometrically by step accumulations. In Fig. 5b, the bifurcation indicator is computed with high accuracy by Taylor series which vanishes at the critical load $\lambda = 20.38$. This value is confirmed by computing the Padé approximants (see Table 2).

These results confirm that the three techniques associating MFS with ANM permit to detect accurately the bifurcation points. This algorithm can be used for complex structural buckling.

8. Conclusion

In this work, we have presented an extended algorithm associating the Method of Fundamental Solutions with the Asymptotic Numerical Method to compute bifurcation points for nonlinear elasticity problems. Three bifurcation indicators have been used. A geometrical indicator permits to localize the bifurcation by observing step accumulations on the solution branches. The second indicator is based on Padé approximants, where the bifurcation point corresponds to the real root of the denominator of the rational fraction. The last one consists in constructing a scalar indicator based on Taylor series that vanishes exactly at the bifurcation points. The effectiveness of these algorithms have been shown throughout two main examples. Work is in progress for other applications in solid and fluid mechanics.

Appendix A

Our study is limited to two-dimensional structures $U \equiv \{U\} = {}^t \langle U_1 \ U_2 \rangle$. Taking into account the non-symmetry of the first Piola-Kirchhoff stress tensor and the symmetry of the second one as well as of the Green-Lagrange strain tensor, we will have $\Pi \equiv \{\Pi\} = {}^t \langle \Pi_{11} \ \Pi_{22} \ \Pi_{12} \ \Pi_{21} \rangle$, $S \equiv \{S\} = {}^t \langle S_{11} \ S_{22} \ S_{12} \rangle$ and $\gamma \equiv \{\gamma\} = {}^t \langle \gamma_{11} \ \gamma_{22} \ \gamma_{12} \rangle$. By introducing the generalized gradient vector $\{\theta\}$ which is written as $\{\theta\} = {}^t \langle U_{1,1} \ U_{1,2} \ U_{2,1} \ U_{2,2} \rangle$, the operators of Eq. (5) are defined in the two-dimensional framework as follows:

$$\begin{cases} \mathcal{L}^\gamma(U) &= [II]\{\theta\} \\ \mathcal{Q}^\gamma(U, U) &= \frac{1}{2}[A(\theta)]\{\theta\} \\ \mathcal{L}^\Pi(S) &= [III]\{S\} \\ \mathcal{Q}^\Pi(U, S) &= [B(\theta)]\{S\} \end{cases} \tag{23}$$

The matrices $[A(\theta)]$, $[B(\theta)]$, $[III]$ and $[II]$ are given by:

$$\begin{aligned} [A(\theta)] &= \begin{bmatrix} U_{1,1} & 0 & U_{2,1} & 0 \\ 0 & U_{1,2} & 0 & U_{2,2} \\ U_{1,2} & U_{1,1} & U_{2,2} & U_{2,1} \end{bmatrix}; [B(\theta)] = \begin{bmatrix} U_{1,1} & 0 & U_{1,2} \\ 0 & U_{2,2} & U_{2,1} \\ 0 & U_{1,2} & U_{1,1} \\ U_{2,1} & 0 & U_{2,2} \end{bmatrix}; \\ [II] &= \begin{bmatrix} 1 & 0 & 0 & 0 \\ 0 & 0 & 0 & 1 \\ 0 & 1 & 1 & 0 \end{bmatrix}; [III] = \begin{bmatrix} 1 & 0 & 0 \\ 0 & 1 & 0 \\ 0 & 0 & 1 \\ 0 & 0 & 1 \end{bmatrix} \end{aligned} \tag{24}$$

Here, $U_{i,j} = \frac{\partial U_i}{\partial x_j}$ ($i, j = 1, 2$) indicates the derivative of the component U_i with respect to the j^{th} variable. The behavior matrix $[C]$ for a homogeneous and isotropic elastic material can be written as follows:

$$[C] = \frac{\bar{E}}{1 - \bar{\nu}^2} \begin{bmatrix} 1 & \bar{\nu} & 0 \\ \bar{\nu} & 1 & 0 \\ 0 & 0 & \frac{1-\bar{\nu}}{2} \end{bmatrix} \tag{25}$$

where $\bar{E} = E$, $\bar{\nu} = \nu$ for the plane stress condition and $\bar{E} = E/(1 - \nu^2)$, $\bar{\nu} = \nu/(1 - \nu^2)$ for the plane strain condition, E and ν are respectively the Young's modulus and the Poisson's coefficient. The operators of Eqs. (8) and (9) are defined as follows:

$$\begin{cases} \mathcal{L}_t^\nabla(U_k) &= [\text{div}] \left(([III] + [B(\theta_0)]) [C] ([II] + [A(\theta_0)]) + [\widehat{S}_0] \right) \{\theta_k\} \\ \mathcal{L}_t^f(U_k) &= [N] \left(([III] + [B(\theta_0)]) [C] ([II] + [A(\theta_0)]) + [\widehat{S}_0] \right) \{\theta_k\} \\ \mathcal{Q}_k^\nabla &= -[\text{div}] \left(([III] + [B(\theta_0)]) [C] \sum_{r=1}^{k-1} \mathcal{Q}^\gamma(U_r, U_{k-r}) + \sum_{r=1}^{k-1} \mathcal{Q}^\Pi(U_r, S_{k-r}) \right) \\ \mathcal{Q}_k^f &= -[N] \left(([III] + [B(\theta_0)]) [C] \sum_{r=1}^{k-1} \mathcal{Q}^\gamma(U_r, U_{k-r}) + \sum_{r=1}^{k-1} \mathcal{Q}^\Pi(U_r, S_{k-r}) \right) \end{cases} \tag{26}$$

the matrix $[\widehat{S}_0]$ contains the stress of the starting solution, defined as:

$$[\widehat{S}_0] = \begin{bmatrix} S_{11}^0 & S_{12}^0 & 0 & 0 \\ 0 & 0 & S_{12}^0 & S_{22}^0 \\ S_{12}^0 & S_{22}^0 & 0 & 0 \\ 0 & 0 & S_{11}^0 & S_{12}^0 \end{bmatrix} \tag{27}$$

The operators $\delta \mathcal{Q}_k^\nabla$ and $\delta \mathcal{Q}_k^f$ of Eq. (16) are defined as follows:

$$\begin{cases} \delta \mathcal{Q}_k^\nabla &= -[\text{div}] \left(2([III] + [B(\theta_0)]) [C] \sum_{r=1}^{k-1} \mathcal{Q}^\gamma(U_r, \delta U_{k-r}) + \sum_{r=1}^{k-1} \mathcal{Q}^\Pi(U_r, \delta S_{k-r}) + \mathcal{Q}^\Pi(\delta U_r, S_{k-r}) \right) \\ \delta \mathcal{Q}_k^f &= -[N] \left(([III] + [B(\theta_0)]) [C] \sum_{r=1}^{k-1} \mathcal{Q}^\gamma(U_r, \delta U_{k-r}) + \sum_{r=1}^{k-1} \mathcal{Q}^\Pi(U_r, \delta S_{k-r}) + \mathcal{Q}^\Pi(\delta U_r, S_{k-r}) \right) \end{cases} \tag{28}$$

References

[1] A. Tri, H. Zahrouni, M. Potier-Ferry, High order continuation algorithm and meshless procedures to solve nonlinear Poisson problems, Eng. Anal. Bound. Elem. 36 (2012) 1705–1714.
 [2] A. Tri, H. Zahrouni, M. Potier-Ferry, Bifurcation indicator based on meshless and asymptotic numerical methods for nonlinear Poisson problems, Numer. Methods Partial Differ. Equ. 30 (2014) 978–993.

- [3] S. Mesmoudi, A. Timesli, B. Braikat, H. Lahmam, H. Zahrouni, A 2D mechanical-thermal coupled model to simulate material mixing observed in friction stir welding process, *Eng. Comput.* 33 (4) (2017) 885–895.
- [4] A. Elhage-Hussein, M. Potier-Ferry, N. Damil, A numerical continuation method based on Padé approximants, *Int. J. Solids Struct.* 37 (46–47) (2000) 6981–7001.
- [5] B. Cochelin, A path-following technique via an asymptotic-numerical method, *Comput. Struct.* 53 (5) (1994) 1181–1192.
- [6] O. Askour, A. Tri, B. Braikat, H. Zahrouni, M. Potier-Ferry, Method of fundamental solutions and high order algorithm to solve nonlinear elastic problems, *Eng. Anal. Bound. Elem.* 89 (2018) 25–35.
- [7] V.D. Kupradze, M.A. Aleksidze, The method of functional equations for the approximate solution of certain boundary value problems, *USSR Comput. Math. Math. Phys.* 4 (4) (1964) 82–126.
- [8] K. Balakrishnan, P.A. Ramachandran, Osculatory interpolation in the method of fundamental solution for nonlinear Poisson problems, *J. Comput. Phys.* 172 (1) (2001) 1–18.
- [9] K. Balakrishnan, R. Sureshkumar, P.A. Ramachandran, An operator splitting-radial basis function method for the solution of transient nonlinear Poisson problems, *Comput. Math. Appl.* 43 (3–5) (2002) 289–304.
- [10] L. Marin, D. Lesnic, The method of fundamental solutions for the Cauchy problem in two-dimensional linear elasticity, *Int. J. Solids Struct.* 41 (13) (2004) 3425–3438.
- [11] A. Karageorghis, D. Lesnic, L. Marin, The method of fundamental solutions for an inverse boundary value problem in static thermo-elasticity, *Comput. Struct.* 135 (2014) 32–39.
- [12] H.J. Al-Gahtani, M. Naffa'a, RBF meshless method for large deflection of thin plates with immovable edges, *Eng. Anal. Bound. Elem.* 33 (2) (2009) 176–183.
- [13] M. Jankowska, J. Kołodziej, A study of elastic-plastic deformation in the plate with the incremental theory and the meshless methods, *J. Mech. Mater. Struct.* 11 (1) (2016) 41–60.
- [14] B. Cochelin, N. Damil, M. Potier-Ferry, *Méthode asymptotique numérique*, Hermès Lavoisier, 2007.
- [15] J.T. Katsikadelis, M.S. Nerantzaki, The boundary element method for nonlinear problems, *Eng. Anal. Bound. Elem.* 23 (5–6) (1999) 365–373.
- [16] T.R. Bridges, L.C. Wrobel, A dual reciprocity formulation for elasticity problems with body forces using augmented thin plate splines, *Commun. Numer. Methods Eng.* 12 (3) (1996) 209–220.